

# Experimental Polymer Bearing Health Estimation and Test Stand Benchmarking for Wave Energy Converters

Michael T. Koopmans<sup>1</sup>, Stephen Meicke<sup>1</sup>, Irem Y. Tumer<sup>1</sup>, Robert Paasch<sup>1</sup>

<sup>1</sup> Oregon State University, Corvallis, OR, 97331, USA

*koopmans@engr.orst.edu*

*meickes@onid.orst.edu*

*irem.tumer@oregonstate.edu*

*paasch@engr.oregonstate.edu*

## ABSTRACT

Ocean waves can provide a renewable and secure energy supply to coastal residents around the world. Yet, to safely harness and convert the available energy, issues such as bearing reliability and maintainability need to be resolved. This paper presents the application of a Prognostics and Health Management (PHM) based research methodology to derive empirical models for estimating the wear of polymer bearings installed on wave energy converters. Forming the foundation of the approach is an applicable wave model, sample data set, and experimental test stand to impose loading conditions similar to that expected in real seas. The resulting wear rates were found to be linear and stable, enabling coarse health estimations of the bearing surface.

## 1. INTRODUCTION

Aggressive development of new energy resources for an ever growing human population is currently underway, and ocean waves have shown promise as a viable source of renewable energy. The interest in offshore power production is due in no small part to the proximity of consumers: over the next 15 years, 75% of the world's population is projected to live within 200 km of the coast (Hinrichsen, 1999), while the worldwide resource has been conservatively estimated to contain 200 - 500 GW of economically extractable energy (Cruz, 2008). Yet, designing, installing, operating, and maintaining systems to harness this renewable energy is an extremely complex problem from multiple standpoints. From an engineer's perspective, the most immediate and challenging problems revolve around device reliability and survivability within the marine environment.

Located in extremely energetic wave climates, a wave energy converter (WEC) is subjected to an array of loads and millions of oscillatory cycles per year. Depending on the device, certain components will deteriorate more rapidly than others, particularly the bearing surfaces that many WEC designs rely upon. Here, prognostic and health management (PHM) techniques can help create a strategy to cultivate information for predicting bearing degradation. These tech-

niques are important because often times the quality of the bearing surface directly affects the total cost of the device in terms not limited to 1) power take-off efficiency, 2) scheduled and/or non-scheduled maintenance, and 3) device survivability. Hence, the success of research efforts to assess and manage WEC reliability remains a critical step to the growth of the ocean renewable energy market.

Therefore, to help contextualize the problem and aid in WEC component-level experiments, system health research methods within the PHM community (Vachtsevanos, Lewis, Roemer, Hess, & Wu, 2006) were sought. A WEC's complexity, although not as involved as other complex systems such as aircraft, automobiles, or a submarine, is intensified with its naturally corrosive, brutal, and immense spectrum of marine operating conditions. Consequently, extensive and efficient use of laboratory experiments is needed to build the marine renewable community's database of seawater-based component life models. To populate this database, an accepted and scalable methodology is needed. This paper explores a proposed PHM research methodology (Uckun, Goebel, & Lucas, 2008) to lay the foundation for an experimental approach to measure bearing wear. More specifically, this study aims to assess the wear characteristics of polymer-based bearings immersed in seawater that are subject to loads and oscillations similar to those experienced by a point absorber WEC in real seas. Our investigation has three goals:

1. Verify and benchmark test stand design and operation for bearing wear measurements
2. Conduct wave energy research following a proposed PHM methodology
3. Present an initial study of polymer bearing health estimation utilizing wear models derived from a set of generalized representative sea states

### 1.1 Main Contributions of the Paper

The work presented here is the beginning of a larger research effort to assess and manage WEC reliability, maintainability, and overall system health using PHM based techniques. Beginning with the bearing design and operating effects, accurate material wear models become critical in determining the efficiency of the device power output. The contributions of this study are itemized as follows:

Michael T. Koopmans et.al. This is an open-access article distributed under the terms of the Creative Commons Attribution 3.0 United States License, which permits unrestricted use, distribution, and reproduction in any medium, provided the original author and source are credited.

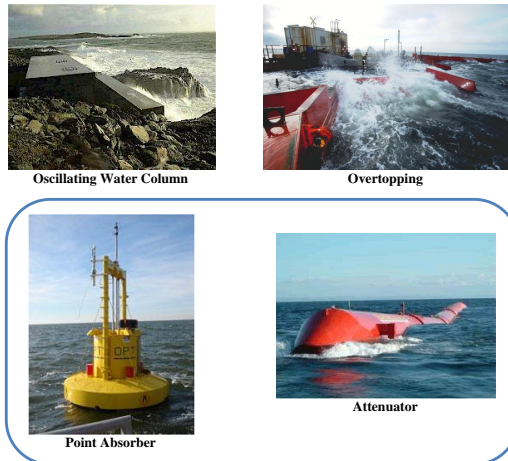


Figure 1: Oscillating wave energy converter devices.

- A PHM based methodology was used to determine polymer bearing wear models with respect to their pressure and velocity parameters in seawater;
- Wave climate load classification was detailed for a point absorber WEC in generalized real seas;
- Cumulative wear of proposed bearing material was estimated for a given month;
- Relevant information was provided to ocean renewable developers and partners to help assess the applicability of the materials and improve the technology;
- An experimental test stand's performance was benchmarked and recommendations were offered for future bearing tests.

## 1.2 Roadmap

The paper will begin with a brief background section, including an introduction to the point absorber WEC, application assumptions, and an overview of the PHM research method. Next, the wave climate and the process used to determine experimental wave cases are discussed, followed by a description of the experimental setup. Results of the bearing wear tests, their implications, and future studies are also presented.

## 2. BACKGROUND

This section provides a brief description of the chosen wave energy converter (WEC), test stand effects, and modeling considerations. To begin, there are generally four main groups of WEC designs: oscillating water columns, overtopping devices, point absorbers, and attenuators (Fig. 1) (Ocean Power Technologies, 2011; Wave Dragon, 2011; Wavegen, 2011). Each device relies on bearings to either support a turbine shaft (water columns and overtopping) or provide a sliding surface on which two large masses can move relative to each other (Yemm, 2003). Specifically, the point absorber and attenuator WECs are designed to harvest the heave motion of a passing wave through their power take-off (linearly or rotationally), where the relative motion of two or more large masses is exploited to generate electricity. Other examples of seawater exposed bearing applications include wind plus wave energy harvesters (Floating Power Plant, 2011) and sea floor based rotational power take-offs (Aquamarine Power, 2011).

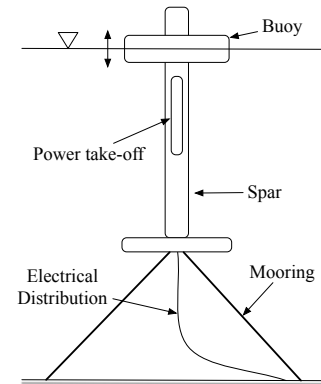


Figure 2: A generic linear power take-off point absorber WEC architecture layout, where relative motion between the buoy and spar provide energy conversion opportunities.

### 2.1 The Point Absorber

Focusing on the point absorber design, the system contains a few core subsystems: power take-off, mooring, structures, control, and distribution (Fig. 2). The device is capable of translating in three degrees: heave (up/down), surge (forward/back), sway (starboard/port) and rotating three degrees about its axis: pitch, yaw, and roll. This investigation will only consider the structures subsystem of a point absorber WEC (buoy and spar) and its heave dynamics with respect to the sea floor. Power take-off, mooring, and control do play very important roles in the loading conditions of the bearing surface, albeit require much more knowledge about the WEC system itself and is not covered in this paper. Essentially, this study assumes one degree of freedom (heave) and a float that is a perfect wave follower. In other words, when solving for the heave dynamics, it will be assumed that as each wave passes, the buoy will travel up and down with the water surface. This relative velocity between buoy and spar is the assumed velocity the bearing surface will experience during operation (i.e., power generation). In storms however, the WEC is most likely not converting energy and may switch to a survivability mode; one possible technique locks the buoy in place to impede system damage.

The bearing subsystem is integrated into the structure of the WEC and provides a surface on which the buoy and spar may move relative to each other. To avoid installing a bearing material sleeve along the entire inner diameter of the buoy, one possible solution lays two to four equally-spaced counterface extrusions around the spar, where they are mated with bearing blocks impregnated within the buoy. Here, the bearing requirements for many WEC technologies demand the surface to be inexpensive, corrosion-resistant, low maintenance, and near-zero friction in a large variety of loading conditions. One proposed solution utilizes a polymer-based approach, similar to those found in current naval designs (Cowper, Kolomojcev, Danahy, & Happe, 2006) and hydropower applications (McCarthy & Glavatskih, 2009; Ren & Muschta, 2010).

This simple polymer-based approach has proven to be beneficial in such applications for its ability to self-lubricate and deposit a transfer film on the counterface, filling in surface asperities, linearizing the wear rate, and even reducing friction in some cases (Wang, Yan, & Xue, 2009). However, water's tendency of inhibiting or wholly preventing transfer film formation is a research topic itself and will only be indi-

rectly addressed in this work. Research regarding wear characterization of polymer journal bearings has been published at various pressures, velocities, and environmental conditions (Ginzburg, Tochil'nikov, Bakhareva, & Kireenko, 2006; Ry-muza, 1990); yet, few studies have been shared with the wave energy community presenting the results of seawater immersion (W.D. Craig, 1964; Tsuyoshi, Kunihiro, Noriyuki, Shozo, & Keisuke, 2005), let alone under pressures and velocities expected to be experienced by WECs (Caraher, Chick, & Mueller, 2008). So, with an immature technology being relied upon by a large complex system, an experimental test stand has been designed and used to procure knowledge about the bearing material's performance characteristics under representative loading conditions.

## 2.2 PHM Based Techniques

As previously mentioned, the research methodology born in the PHM community provides a good platform on which test stand research can be integrated into a larger, more comprehensive effort to assess system health. A general outline is shown in Fig. 3, where the path to implementing and relying upon a prognostic solution begins first with high-level system requirements (health predictions for subsystems and/or the system itself) that define the subsequent metric, fault, and sensor selection process. Next, the third step determines the most appropriate approach in terms of desired performance, available resources, and acceptable uncertainty to satisfy the component-level predictions. Here the proper number of samples to sacrifice for an accurate inference is also set. The fourth step ascertains the test scenarios, design of experiments, and data collection, while the fifth step is dedicated to building models and remaining useful life algorithms for nominal and faulted conditions. The last two steps encompass the health estimation and actual usage comparisons, in addition to the verification and validation sequence. A good application of the entire PHM research methodology was presented in estimating battery capacitance over time using high quality test chambers (Goebel, Saha, Saxena, Celaya, & Christophersen, 2008). For this work however, only a few steps of the methodology are addressed for estimating WEC bearing wear. Knowing that it would be useful to predict bearing wear in extreme marine conditions, the initial strategy to determine adequate experimental conditions and data collection procedures is described in addition to how the test stand itself contributes to the main goals of this investigation.

## 2.3 Test Stand Considerations

The test stand design and operation are critical to the validity of the empirical bearing wear models. Many interested researchers have built test stands to measure the degradation of particular components, including batteries (Saha, Goebel, Poll, & Christophersen, 2009), actuators (Balaban et al., 2010; Bodden, Clements, Schley, & Jenney, 2007), and polymer bearings (Gawarkiewicz & Wasilczuk, 2007). The particular test stand employed for the experiments presented in this paper is a modified version of American Society for Testing and Materials' (ASTM) standard test for ranking plastic resistance (ASTM, 2009), where the major changes to the standard include an oscillatory velocity, varying loads, and immersing the sample in seawater. Being a relatively new field of research, a lack of verification and validation of the modified test stand contributes to the uncertainty of the results. A goal of this work is to verify and benchmark test stand design and operation, ensuring the bearing wear measured repeatedly and accurately reflects imposed loading conditions.

## 2.4 Modeling Considerations

When investigating and modeling polymer bearing wear, it is important to note that multiple factors contribute to the wear rate. A polymer bearing / counterface tribosystem failure modes and effects analysis may contain only a few failure causes, where a primary failure would be the direct result of the physical amount of bearing material removed, and secondary failures may be attributed to biofouling or sediment-rich seawater. This study only covers the primary failure (wear) and does not address secondary failures. Also, a wear estimation is considered synonymous with a bearing health estimation because the bearing's ability to perform as designed is assumed to be directly attributed to the physical amount of material remaining in place.

One must also consider the naturally stochastic ocean waves. Their modeling effort has been well documented (Tucker & Pitt, 2001; Holthuijsen, 2007; Young, 1999) and the trade-off between the relevance of a higher fidelity numerical model and a closed-form solution must be done. For this work, the mapping of sea state to bearing pressure and velocity will be solved analytically with several conservative assumptions (e.g., linear waves, buoy / spar dynamics) that serve well as an initial attempt to assess the applicability of this research.

## 3. THE WAVE CLIMATE

Within the fourth step of the PHM methodology, expected sea states are sought to derive the pressures and velocities experienced by the bearing surface. In order to choose experimental cases representative of WEC oscillations and loads, a wave climate comparable to permitted sites was chosen (FERC, 2011). A wave climate is defined here as the aggregation of all the reported wave measurements taken at a specific location. The most accessible sources for past wave climate information include the Coastal Data Information Program (CDIP, 2011) and the National Data Buoy Center (NDBC, 2011) who manages a worldwide buoy network. A buoy of particular interest for its similarities to a potential WEC installation (proximity to coast / large population areas, consistent and predictable wave energy) is located 15.5 nautical miles northwest of Winchester Bay, Oregon (NDBC station ID: 46229), where the water depth is 186 meters and the buoy is assumed to be a perfect wave follower.

### 3.1 Wave Data

Wave information is often reported in the frequency domain as a wave spectrum, where, for each frequency and respective bandwidth, the energy or wave energy density is registered (Tucker, 1991). Other parameters included in the report can denote the wave direction, depending on the buoy. Much more wave data is also available apart from the spectral information, including the raw time series values, which is used for much higher fidelity WEC modeling. For the purpose of this study however, only two parameters were used in defining the wave climate: significant wave height ( $H_s$ ) and dominant wave period ( $T_D$ ). The significant wave height (in meters) is the average of the highest one-third of all the wave heights encountered during the 20 minute sampling period. The dominant wave period (in seconds) is the period with maximum wave energy as taken from the wave spectrum over the sampling period (Steele & Mettlach, 1993).

### 3.2 The Sample Data Set

Significant wave heights and dominant wave periods were taken for years 2005 - 2010 (NDBC, 2011). Reporting data

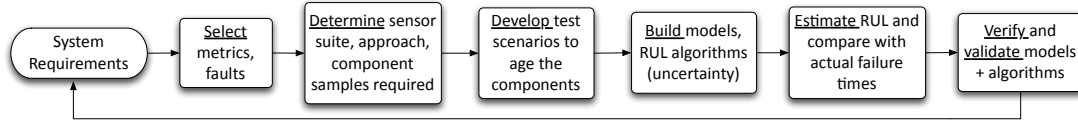


Figure 3: A universal PHM research methodology.

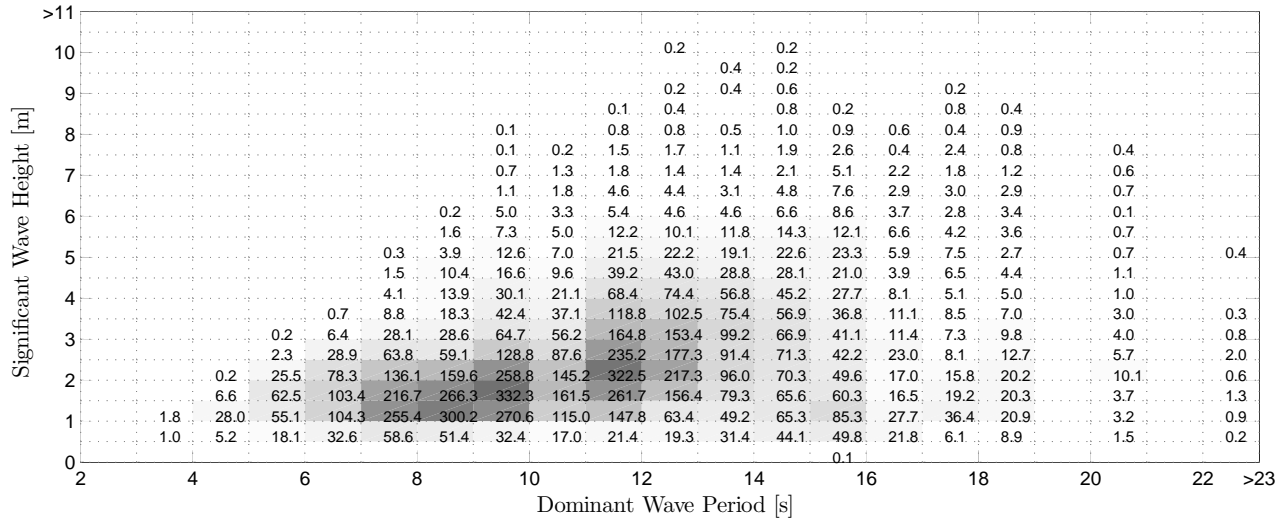


Figure 4: The total wave climate, where each bin contains the average number of hours for each sea state for an average year during the past six years (2005 - 2010).

every hour until the end of January 2008, the sampling rate was increased to every half hour. The entire data set is not complete, as some data points are erroneous (e.g.,  $H_s = T_D = 99$ ) or absent altogether. To include some of these reports in the sample data set, the erroneous points were replaced with the average of their nearest neighbors, whereas the absent points were left out of the averaging process. No weighting was installed to unbias the months with more hours reported over the months with lesser hours reported. There were four major gaps in the data, where no reports were given for the following dates: 1/1/05 - 4/1/05, 2/25/06 - 5/11/06, 5/29/06 - 7/13/06, and 3/16/09 - 4/1/09. Three of the four gaps occur in the spring and summer, while the largest consecutive gap occurs in the winter. This may be due to a more energetic sea state during these months causing system failures. Overall, the six years of coverage yielded only 5.06 years of data. This fact affects the total wave climate picture in terms of number of hours per particular sea state, but for the purpose of choosing test wave parameters, it is not foreseen to affect the results of this study. Therefore, the data set from which the experimental cases were determined can be seen in Fig. 4, where each bin covers one second wave periods and half meter wave heights with the average number of hours reported for that bin over the measured time period displayed in the plot. The most common sea state was a 9 - 10 second period and 1.5 - 2.0 meter wave height, accounting for approximately 3.8% of the yearly total.

### 3.3 Choosing Experimental Cases

In order to effectively achieve a spread of experimental cases, the wave period distribution was analyzed as shown in Fig. 5 while the wave heights were taken at each period interval. An

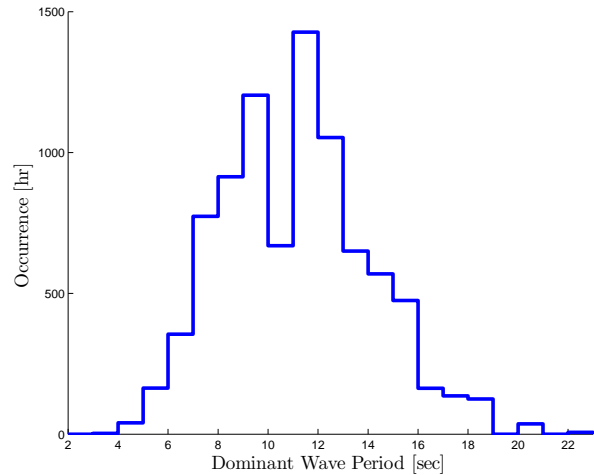


Figure 5: Wave period distribution over the entire climate data set, with an average of 10.89 sec and a standard deviation of 2.95 sec.

interval is defined here as a particular one second period bin determined by the average and standard deviation of the cumulative wave period distribution where the column of wave heights is then sampled to find the exact experimental case (i.e.,  $H$  and  $T$ ). For the test period of 10.89 sec, the 10 - 11 sec period bin was analyzed (Fig. 6), as were the other three test period bins (7 - 8 sec, 13 - 14 sec, and 16 - 17 sec) to achieve all four experimental cases (Tbl. 1).

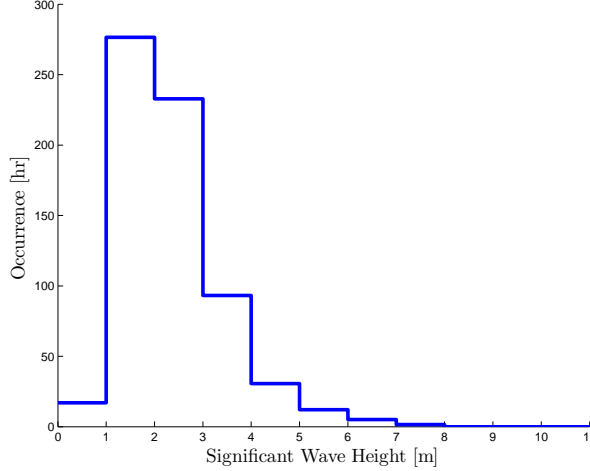


Figure 6: Distributions of significant wave heights for the 10 -11 sec period bin with an average of 2.3 m and a standard deviation of 1.0 m.

Exp. Case	$T$ (s)	$H$ (m)
1	10.89	2.31
2	13.84	5.51
3	16.79	2.92
4	7.95	1.74

Table 1: Chosen test wave heights and periods.

#### 4. EXPERIMENTAL DESIGN

This section explains the design decisions and limitations behind the bearing wear experiments and their corresponding parameters, including the bearing health estimation algorithm (addressing step three and parts of step five of the PHM methodology). Knowing the experimental wave parameters, the calculation of pressures and velocities at the surface of interest is described. First, a description of the procedure to compute the loading condition input for each bearing wear experiment is presented, followed by a table containing each experimental case parameter. Many assumptions support the closed-form procedure taken in this paper and will be discussed as they are applied.

##### 4.1 Wave Modeling and Force Calculation

First, the wave experienced by the WEC is classified using four main parameters: water depth  $h$ , wave height  $H$ , wave length  $L$ , and wave period  $T$  (Fig. 7), where  $\eta$  describes the wave surface elevation in terms of  $x$  and  $t$  while having a value of  $z$  meters. The wave itself is assumed to be harmonic and linear (or regular); other wave classifications include irregular, ocean, and stochastic ocean waves (Ochi, 1998). Generalizing the sea state under linear wave theory is the most basic approach to modeling the ocean surface and is deemed appropriate for this initial study.

The generalization assumes the fluid to be incompressible and inviscid (irrotational), enabling the local water particle velocities to be solved explicitly and facilitating the use of Morison's equation (Dean & Dalrymple, 1991). In a typical design, a software program is tasked with computing the

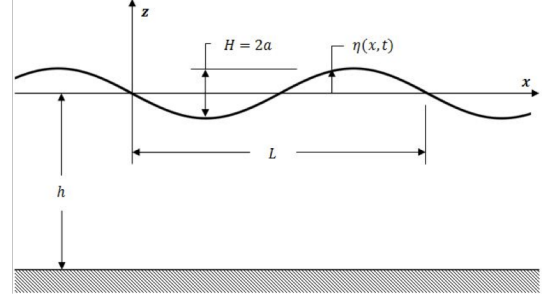


Figure 7: A regular two dimensional wave with relevant parameters and coordinate system shown.

structural loading (e.g., AQWA, WAMIT). However, in our case, the Morison equation will be shown as an initial approach to calculate bearing pressure.

Next, assuming an intermediate water depth, the wave length is solved numerically using Eq. 1, where  $g$  is the acceleration due to gravity. A water depth of 91.4 meters was used in this study to mimic Oregon sites where WEC developers currently hold permits (FERC, 2011).

$$L = \frac{g}{2\pi} T^2 \tanh \frac{2\pi h}{L} \quad (1)$$

The wave length can be verified for use in an intermediate water depth by checking the inequality (Eq. 2), where the wave number is  $k = \frac{2\pi}{L}$ . When calculating a  $kh$  scalar towards the lower or upper extremes, a shallow or deep water assumption, respectively, would instead prove more accurate.

$$\frac{\pi}{10} < kh < \pi \quad (2)$$

Next, the water surface displacement,  $\eta$ , is given in Eq. 3, where  $\sigma = \frac{2\pi}{T}$  and its correlated velocity potential,  $\phi$ , is given in Eq. 4.

$$\eta(x, t) = \frac{H}{2} \cos(kx - \sigma t) \quad (3)$$

$$\phi = -\frac{gH}{2\sigma} \frac{\cosh k(h+z)}{\cosh kh} \sin(kx - \sigma t) \quad (4)$$

The closed-form velocity potential allows for the calculation of horizontal ( $-\frac{\partial\phi}{\partial x}$ ) and vertical ( $-\frac{\partial\phi}{\partial z}$ ) water particle velocities, which can be seen in Eq. 5 and Eq. 6, respectively.

$$u = -\frac{\partial\phi}{\partial x} = \frac{gHk}{2\sigma} \frac{\cosh k(h+z)}{\cosh kh} \cos(kx - \sigma t) \quad (5)$$

$$v = -\frac{\partial\phi}{\partial z} = \frac{H\sigma}{2} \frac{\sinh k(h+z)}{\sinh kh} \sin(kx - \sigma t) \quad (6)$$

The local horizontal acceleration is shown in Eq. 7.

$$\frac{\partial u}{\partial t} = \frac{H\sigma^2}{2} \frac{\cosh k(h+z)}{\sinh kh} \sin(kx - \sigma t) \quad (7)$$

Using these equations, an estimation of the horizontal force imposed on the buoy by a passing wave can be computed.

Typically used to design and estimate loads on columns embedded in the sea floor, Morison's equation (Eq. 8) can be employed during conceptual WEC design for computing the horizontal wave force imparted on the device by a passing regular wave (Morison, O'Brien, Johnson, & Schaaf, 1950).

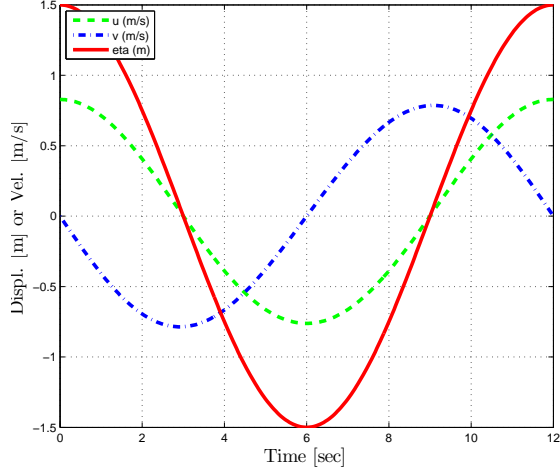


Figure 8: Example surface displacement and corresponding water particle velocities for a  $H = 3$  m,  $T = 12$  sec wave.

The equation is composed of two elements, the first captures the drag forces and the second captures the inertial forces,

$$F(z) = \frac{1}{2} C_D \rho D u |u| + C_M \rho V \frac{Du}{Dt} \quad (8)$$

where  $C_D$ ,  $C_M$ ,  $\rho$ ,  $D$ , and  $V$  represent the drag & inertial coefficients, seawater density ( $1025 \frac{\text{kg}}{\text{m}^3}$ ), buoy diameter, and buoy volume. Ultimately integrated over a water depth with respect to  $z$ , total horizontal force is represented in Eq. 9,

$$F_x = \int_a^b F(z) dz \quad (9)$$

where  $b$  is usually the water displacement ( $\eta$ ), and  $a$  is some value in the vertical length ( $z$ ) of the geometry. For example, if  $a = -h$ , the force would integrate over a continuous column to the sea floor. The aggregation of Eqs. 3 - 9 can be viewed in Fig. 8 and Fig. 9, where the parameters of a  $H = 3$  m,  $T = 12$  sec wave are plotted implementing the zero crossing method.

## 4.2 Experimental Case Parameters

Incorporating the above wave model, chosen wave heights and periods, and force calculations, the experiment case parameters can now be set (Tbl. 2). To reiterate, the experimental cases represent a first attempt at a sample set of representative wave parameters to classify polymer bearing wear during WEC operation. The third column states the maximum velocity the counterface experiences during the oscillatory profile (i.e., Eq. 6). Next, geometric assumptions that enable a specific velocity and pressure to be applied during wear tests are held and explained as follows. A buoy diameter of 11 m was used in the Morison force calculation while the force was integrated over a depth of 1.5 m. This depth was chosen based off the assumed buoy height (1.5 m) and assuming the buoy was fully submerged throughout the length of the passing wave. Next, knowing linear wave theory was being utilized, the drag and inertial coefficients were taken as 1.3 and 2.0, respectively (Agerschou & Edens, 1965). The bearing pressure was computed using the wave force calculation and an assumed bearing area of  $0.232 \text{ m}^2$ . This particular

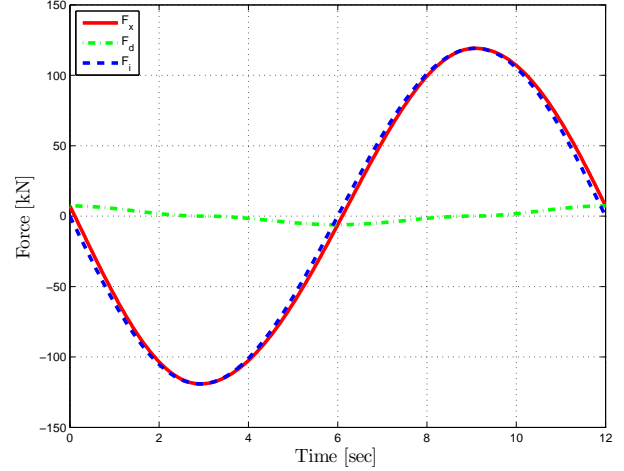


Figure 9: Example force oscillation imposed on the buoy by a passing  $H = 3$  m,  $T = 12$  sec wave, where  $F_d$  and  $F_i$  represent the individual components of  $F_x$ : the drag and inertial forces, respectively. The actual normal force applied to bearing sample was taken as the root mean squared value of the maximum  $F_x$  due to test stand limitations.

area was chosen as a conservative estimate of the total bearing area and set the active bearing pressure below the bearing manufacturer's recommendations.

The final parameter set for the wear testing experiments was the number of runs for each experiment case. Using the operating characteristic (OC) curve to minimize the type II error, Eq. 3 was implemented (Montgomery, 2009),

$$\Phi^2 = \frac{nD^2}{2a\sigma^2} \quad (10)$$

where  $\Phi$  and  $\beta$  (probability of type II error) make up the OC curve  $x$  and  $y$  parameters. Further,  $n$  is the number of runs for each test climate,  $D$  is the difference between two treatment means desired to be detected (0.5),  $a$  is the number of experimental cases (4), and  $\sigma$  is the assumed maximum standard deviation of wear rate at any power level (0.1). These values were based on previous wear studies completed. Tbl. 3 shows the results of checking various sample sizes and it was decided due to the infancy of this research that a probability of 0.85 would be adequate for detecting a difference in wear means ( $D$ ) for separate experiment cases. Consequently, three test runs were specified for each experimental case.

$n$	$\Phi^2$	$\Phi$	$a(n-1)$	$\beta$	Power ( $1-\beta$ )
2	6.3	2.5	4	0.5	0.5
3	9.3	3.0	8	0.15	0.85
4	12.5	3.5	12	0.01	0.99

Table 3: Determining each experimental case's sample size using the operational characteristic curves with  $\alpha = 0.01$ .

## 4.3 Bearing Health Estimation

Once the bearing wear experiments have concluded, the post-processing of the raw linear variable differential transformer

Exp. Case	$T$ (s)	$H$ (m)	$\nu_{\max}$ (m/s)	$F_{\text{rms}}$ (kN)	$P$ (kPa)	$kh$
1	10.89	2.31	0.66	78	334	3.1
2	13.84	5.51	1.25	120	500	2.0
3	16.79	2.92	0.55	47	202	1.4
4	7.95	1.74	0.69	108	445	5.8

Table 2: Experiment Case Parameters

(LVDT) measurements should ideally indicate a linear and stable wear rate. Under these circumstances, the wear models can be pieced together to create a cumulative data driven life model of the bearing surface. This inference allows ocean renewable developers the capability to predict the bearing's health after some length of time. For example, if the life model indicates the amount of bearing material departed is approaching a critical threshold, then operators and maintainers can make informed decisions. Given enough time, the repairs could be scheduled to minimize the cost associated with servicing the bearings. It is important to note that the prediction accuracy of the bearing health estimation is directly attributed to wear model quality and its associated experimental design.

In order to quantify the raw bearing wear in a format applicable to wear predictions, the recorded vertical wear from the LVDT is multiplied by the constant contact area to form the total volumetric wear for the sample seen in Eq. 11,

$$V = 2wrq \sin^{-1}\left(\frac{l}{2r}\right) \quad (11)$$

where  $w$  is the vertical wear,  $r$  is the counterface outer radius,  $l$  is the sample length, and  $q$  is the sample width (all variables in mm). To avoid biasing the wear estimate to focus on force or distance or time alone, a specific wear rate variable is used (Eq. 12),

$$V = eFs \quad (12)$$

where  $V$  is the total volumetric wear ( $\text{mm}^3$ ),  $e$  is the specific wear rate ( $\frac{\text{mm}^3}{\text{Nm}}$ ),  $F$  is the normal load (N), and  $s$  is the sliding distance (m). Solving for  $e$  using the stable portion of the wear plot, a set of specific wear rates are then available to the user for calculating volumetric wear of the bearing during different climates than those tested in the experiment. Assuming the worst case scenario for the specific wear rate model formulation, forces and sliding distances are derived for each particular hour of reported wave parameters. The cumulative volumetric bearing wear is tracked using Eq. 13,

$$\sum_{i=0}^m V_i c_i \quad (13)$$

where  $i$  is the bin index (wave height and period),  $m$  is the number of discrete sea states reported during the time interval,  $V$  is the volumetric wear associated with a particular bin and  $c$  is the total number of hours the WEC experienced seas classified to the particular bin. This purely data driven model would preferably be used in parallel with the wave climate in Fig. 4 and although relatively elementary, could be enormously useful in estimating the overall bearing health, while further informing WEC design, operation, and maintenance decisions.

## 5. EXPERIMENTAL SETUP

This section describes the bearing material and its mating counterface used during this study - addressing step four of the PHM methodology. The test stand is also shown and the procedure to measure bearing wear is described.

### 5.1 Bearing Material

Each bearing sample was machined out of disks (with an inner radius equal to the counterface) 6.40 mm in width into sections of 15.85 mm in length and approximately 10 mm in height. The Thordon SXL bearing material was used throughout the study (Thordon, 2011). Each bearing sample was cleaned with methanol prior to each test to guard against any incidental debris from contaminating the experiment.

### 5.2 Counterface

Two identical 316 stainless steel counterfaces were used during testing, each with a diameter of 63.5 mm (derived from the rpm limit of the motor so as to maximize the range of test surface velocities) as seen in Fig. 10. Before and after each test run, the surface roughness of the counterface was measured using a Mitutoyo surface roughness tester in an attempt to determine any transfer of material to the counterface. As per design recommendations from the manufacturer, the counterface surface roughness was made to be less than  $0.8 \mu\text{m}$  Ra before each test. In an effort to allow for better mechanical bonding of the polymer, roughening was completed perpendicular to the direction of rotation (Marcus, Ball, & Allen, 1991). The roughness measurements were taken in parallel to the direction of rotation at three different points along the width of the counterface and six different section widths around the circle. Prior to each test, the counterface was also thoroughly cleaned with methanol.

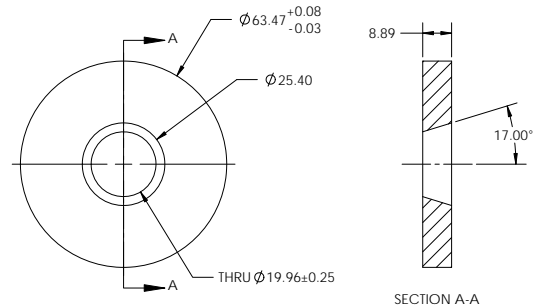


Figure 10: Counterface dimensions.

### 5.3 Test Stand

Implementing a testing method derived from the ASTM G176-03 standard (ASTM, 2009) for ranking wear resistance

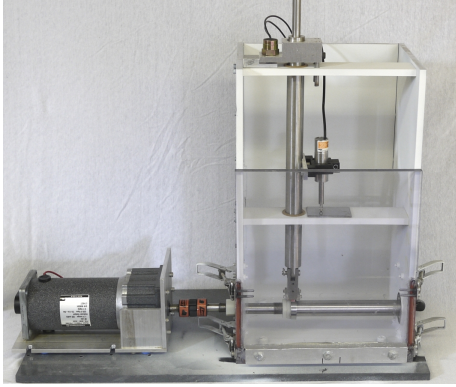


Figure 11: The bearing wear test stand.

of plastic bearings, the test stand can be seen in Fig. 11. Modifications to the setup have been made to allow for complete immersion of both the bearing sample and counterface in seawater. A procedure to run a bearing wear test follows:

1. Empty all seawater from reservoir and wash out with freshwater, lightly touching the counterface (remove salt, but not the transferred bearing material) and remove bearing sample.
2. Remove the counterface from drive shaft, air dry, and measure surface roughness.
3. Take the second, prepped counterface and couple to drive shaft, ensuring minimum change in deflection of the surface during rotation. The authors recommend using a dial indicator to measure this deflection.
4. Set the new, prepared bearing material in place, load mass on vertical shaft, latch front plate, fill reservoir, input test parameters to software, and begin test.

The removable counterface is held in place with two plastic nuts on a stainless steel drive shaft directly coupled to a DC brushed motor. A  $0.5 \mu\text{m}$  resolution LVDT was tasked with measuring the vertical wear of the bearing sample while linked to the vertical shaft responsible for holding the mass load in place. The drive shaft and all connecting parts were cleaned with methanol prior to each test. The seawater used during testing is seawater filtered to  $50 \mu\text{m}$ , taken from Yaquina Bay in Newport, Oregon.

A National Instruments cRIO unit was programmed to control motor velocity using the LabVIEW interface and shaft encoder relaying speed information. The bearing samples were subjected to sinusoidal velocity profiles ( $\nu$ ) oscillating at their specified frequency ( $\frac{1}{T}$ ) and each wear test was run for 20 hours with no intermittent stops. In order to determine the correct mass to load the sample, the test climate pressure ( $P$ ) was multiplied by the bearing sample projected area and divided by the gravity constant,  $g$ .

## 6. RESULTS

This section presents the results of all twelve wear tests, grouped into their four respective experiment cases, followed by the specific wear rate model formulation, a month long bearing health estimation, and the corresponding before and after counterface surface roughness measurements. The raw LVDT readout was smoothed for graphing purposes. Each wear plot contains two x-axes: sliding distance (computed

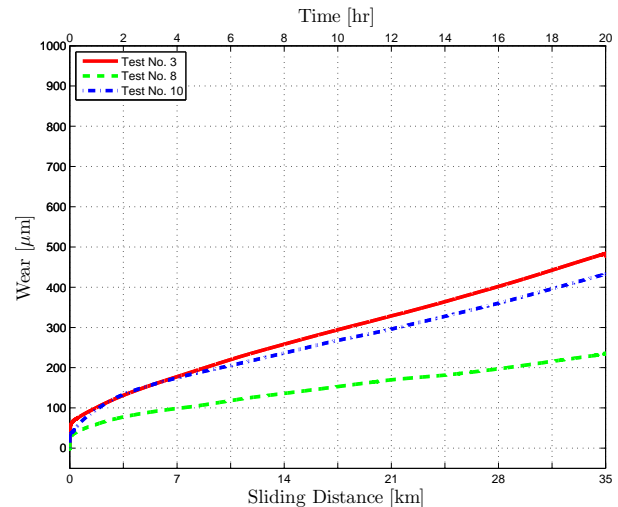


Figure 12: Experiment case one, pressure = 334 kPa, maximum surface velocity = 0.66 m/s, mass = 3.382 kg.

from oscillation frequency, amplitude, and counterface radius) and time (each wear test was 20 hours long). The first case is shown in Fig. 12, while the second, third, and fourth cases are shown in Figs. 13 - 15, respectively. The plots show the highest pressure resulted in the highest wear rate, while the lowest pressure resulted in the lowest wear rate, as expected. And for the majority of test runs, similar patterns exist within each experimental case. However, test run number twelve is an anomaly: around four seven, the wear measurement diverges and increases 350% less than the previous two test runs. Another test run that is unlike its counterparts is number eight, where its wear measurements are offset 50 - 100% less than complementary tests three and ten.

Next, to ensure wear is linear with respect to time and distance, hour six to twenty was set as the stable portion of the wear plot for all test runs. Analyzing this segment, a vertical bearing wear measurement can be used to derive the total volumetric wear and specific wear rate for each test run. Here the results can be seen in Fig. 16, where the dotted line represents a worst case scenario specific wear rate model. For a month long wear estimation, the specific wear rate model was used, where the volumetric wear for each hour of reported wave data was calculated using 1) a specific wear rate,  $e$ , from the model, 2) a normal force,  $F$ , derived from Morison's equation, and 3) a sliding distance,  $s$ , derived from the particular climate's reported wave parameters. For the month of January 2011, a total of 4.5 mm was estimated to have been lost during the theoretical point absorber WEC operation (Fig. 17). Additional information was recorded before and after each test run that included the counterface surface roughness measurements (Tbl. 4).

## 7. DISCUSSION

Upon completing the experiments for this study, the wear plots show the bearing material's performance is dependent on a few external factors including, a direct correlation with the loading conditions and a peculiar association with counterface preparation. The test stand was shown to operate reliably throughout the investigation, however it too affects the wear rate indirectly through load application and velocity control attributes. Further exploring the findings, this section

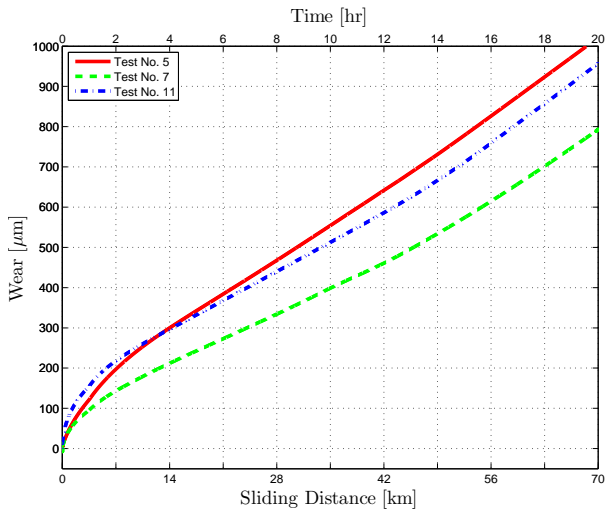


Figure 13: Experiment case two, pressure = 500 kPa, maximum surface velocity = 0.1.25 m/s, mass = 5.000 kg.

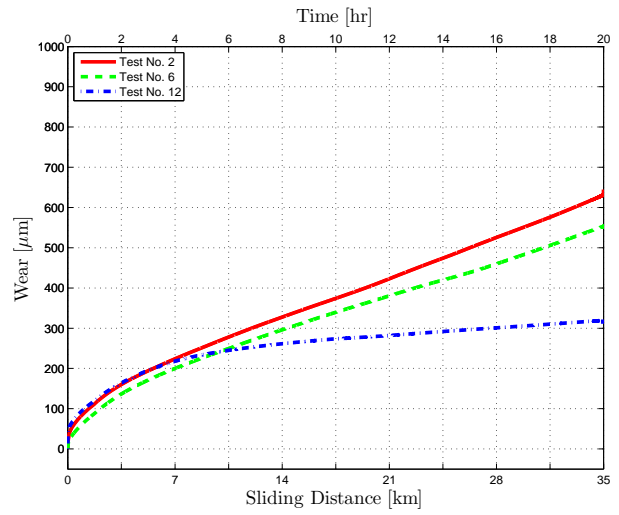


Figure 15: Experiment case four, pressure = 445 kPa, maximum surface velocity = 0.69 m/s, mass = 4.442 kg.

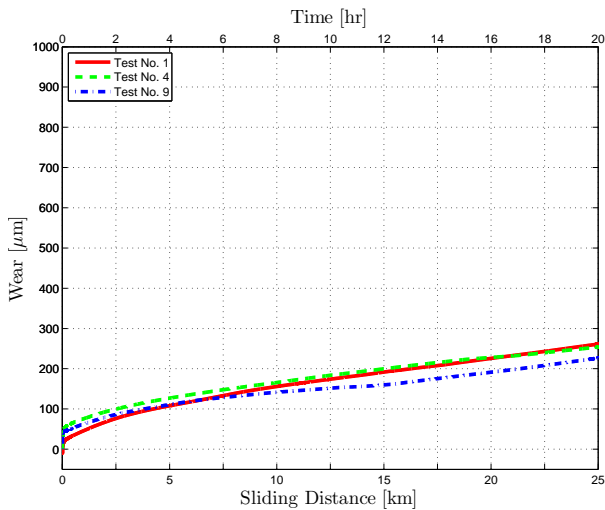


Figure 14: Experiment case three, pressure = 202 kPa, maximum surface velocity = 0.55 m/s, mass = 2.045 kg.

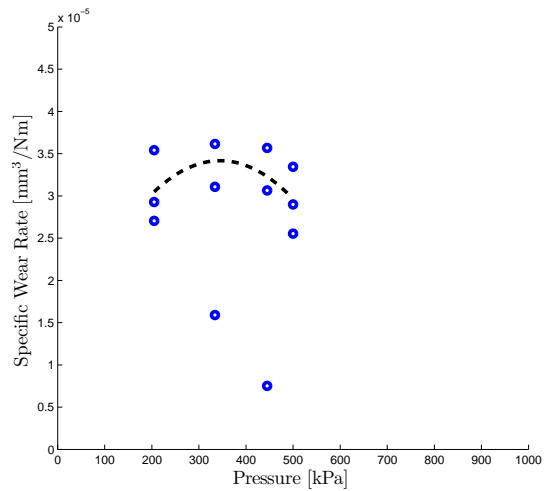


Figure 16: Specific wear rates plotted vs. applied bearing pressure for all twelve test runs with the conservative model overlay (dotted line).

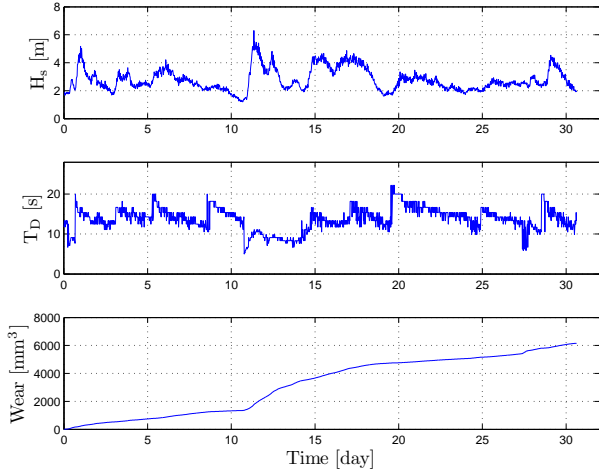


Figure 17: An example wear estimation for the month of January 2011.

Exp. Case	Test No.	Rate ( $\frac{\mu\text{m}}{\text{hr}}$ )	Before ( $\mu\text{m Ra}$ )	After ( $\mu\text{m Ra}$ )
1	3	18	.58 .69 .48	.71 .84 .56
	8	8	.61 .71 .48	.61 .79 .46
	10	16	.56 .69 .43	.53 .71 .38
2	5	45	.66 .81 .51	.63 .79 .41
	7	37	.61 .76 .53	.51 .64 .43
	11	42	.51 .58 .41	.48 .61 .33
3	1	9	.69 .76 .51	.58 .74 .43
	4	7	.69 .74 .58	.69 .79 .58
	9	8	.53 .69 .46	.53 .66 .41
4	2	25	.74 .79 .69	.64 .74 .58
	6	21	.66 .76 .58	.71 .94 .51
	12	5	.61 .71 .53	.56 .69 .43

Table 4: Stable wear rates for each test run and their corresponding before and after surface roughness measurements (average, maximum, minimum).

discusses several factors contributing to the uncertainty in the results. Topics affecting the accuracy of the prediction include the effect of counterface surface roughness, wave modeling, wear data quality, and test stand effects.

### 7.1 Effect of Counterface Roughness

To begin, the effect of surface roughness on the stable wear rate is plainly apparent and as one would expect, a higher roughness generally yields a higher wear rate. Observing experiment case four in particular, test twelve yielded a stable wear rate 4 - 5 times smaller with a pre-test surface roughness less than  $0.06 \mu\text{m}$  smoother than test two or six. Perhaps this result is specific to the experiment (relatively high pressure and frequency oscillation) as the difference between pre-test roughness measurements for experiment cases two and three are similar, yet their subsequent stable wear rates are analogous. It should be noted that there are limits as to how smooth the initial counterface can be as one study showed a roughness of  $0.03 \mu\text{m}$  increased the wear rate by 33 times (Marcus & Allen, 1994). Experiment case one and four both contain a test run dissimilar to the others while their pre-test roughness measurement differences are negligible, indicating that there may be some other factor affecting the results and warranting more experiments.

From previous experience, the bearing material studied exhibited an unusually higher wear rate for their respective loading conditions in the majority of test runs. Acknowledging the customization of the experimental design and operation, the obvious absence of a transfer film may indicate the need for a better application of pressure and velocity to the bearing sample itself via a different test stand design and/or operation.

### 7.2 Wave Modeling

Second, the method of wave modeling used in this investigation assumes a regular wave, which is not an accurate representation of real seas. Propagating linear waves and the assumption of the buoy being a perfect wave follower are likely the most influential assumptions within this study. The most rigorous of ocean wave modeling efforts solve the Navier Stokes non-linear differential equation for velocities and pressure fields, yet is only suggested for higher fidelity investigations. However, the success of applying the often used principle of superposition (as many frequency domain wave models do) to the wear rates remains to be seen given the limitations of linear wave theory (Young, 1999). Another, more promising strategy would be to utilize the WEC dynamics derived from previous modeling efforts (Ruehl, Brekken, Bosma, & Paasch, 2010).

Further, choosing NDBC 46229 as the source of ocean surface measurements was designed to allow researchers the freedom of employing either a time or frequency domain based approach. Also, for a more complete input to the wave climate, the authors suggest employing a method that explicitly presents representative wave spectra (Lenee-Bluhm, 2010).

### 7.3 Wear Data Quality and Health Estimations

Third, the health estimation, however unrefined, was possible because of quality wear data. The empirical models yielded few extraordinary anomalies and provided a good basis for regression and validation of the sample size suggestion. Applying the wear algorithm, approximately  $6000 \text{ mm}^3$ , or 4.5 mm of bearing material was estimated to be lost during the month long WEC operation. This initial estimate is quite large and

could be attributed to several factors, including the material itself, the loading conditions chosen, the load application via the test stand's design and operation, and/or the counterface's surface roughness.

Also, a method for how to rectify the fact that wear rates do not exist for each bin within the wave climate has yet to be developed and would constitute a very interesting future work. Although the experiments do not change parameters during the 20 hour tests, future work would require the programming of varying parameters, resulting in more accurate loading conditions. Also, some of the next steps in this research would apply more advanced aspects of PHM by incorporating uncertainty assessment (Tang, Kacprzynski, Goebel, & Vachtsevanos, 2008) and prognostic evaluation (Saxena et al., 2008).

#### 7.4 Test Stand Effects

Fourth, the effect of the test stand on the bearing experiments is inherent in the wear data, so only by modifying the test stand and running the same experiments would the effect be measurable. During testing, the motor was observed to jerk near the crest and trough of the sinusoid velocity profile, indicating poor torque control. This phenomenon occurred with greater intensity during experimental cases with higher pressures. To solve this problem, a torque sensor and high torque motor would be ideal additions to accurately and smoothly follow the desired velocity profile. Other test stand modifications to produce more accurate results would be the integration of a varying pressure function and time domain velocity profile. Currently, the test stand is limited to constant force application and only after running these initial experiments has it become readily obvious that the test stand is not capable of accurately recreating loading conditions that a bearing sample would see in the field - a much smoother control of the counterface velocity profile is required.

#### 8. CONCLUSION

Twelve bearing wear experiments were conducted using a simplified wave model coupled with an average sea climate to derive representative loading conditions for polymer bearings installed on a point-absorbing WEC. Following a PHM based research method, a stable and linear wear rate was established for each experiment, leading to the use of empirical methods for estimating bearing wear. Not only was essential information gained regarding the limits of the experiments, but the actual research methodology as well. Much work remains, albeit progress was made towards careful benchmarking of the test stand and successful employment of PHM research tenets.

As a note, PHM is often an afterthought in complex system design because of many unanswered questions regarding prognostic requirements and their resulting validation sequence (Ferrell, 2010). This research focused on one component of the WEC and illuminated experimental attributes critical to its life predictions, even as developers work to install production-level devices where bearing health estimation may be the lowest of priorities. Promoting a scalable and technically sound approach to classifying WEC bearing performance early in the industrial development is significant, as benefits can quickly materialize for all parties.

#### ACKNOWLEDGMENTS

The authors wish to thank Thordon Bearings for supplying the bearing samples used in this study.

#### NOMENCLATURE

PHM	Prognostics and Health Management
WEC	Wave Energy Converter
$T_D$	dominant wave period
$H_s$	significant wave height
$\eta$	water surface displacement, a function of $x$ and $t$
$k$	wave number
$\phi$	water particle velocity potential
$F_x$	horizontal force imposed on buoy by passing wave
$e$	specific wear rate
$i$	bin index (wave height and wave period)
$V_i$	volumetric wear
$c_i$	total bin index hours

#### REFERENCES

- Agerschou, H., & Edens, J. (1965). Fifth and First Order Wave - Force Coefficients for Cylindrical Piles. In *ASCE Coastal Engr. Speciality Conf. Ch. 10. pp. 239*.
- Aquamarine Power. (2011). (<http://www.aquamarinepower.com/>)
- ASTM. (2009). G176 - 03(2009) Standard Test Method for Ranking Resistance of Plastics to Sliding Wear using Block-on-Ring Wear Test, Cumulative Wear Method. (<http://www.astm.org/Standards/G176.htm>)
- Balaban, E., Saxena, A., Narasimhan, S., Roychoudhury, I., Goebel, K. F., & Koopmans, M. T. (2010). Airborne Electro-Mechanical Actuator Test Stand for Development of Prognostic Health Management Systems. In *Annual Conference of the Prognostics and Health Management Society*.
- Bodden, D. S., Clements, N. S., Schley, B., & Jenney, G. D. (2007). Seeded Failure Testing and Analysis of an Electro-mechanical Actuator. In *IEEE*.
- Caraher, S., Chick, J., & Mueller, M. (2008). Investigation into Contact and Hydrostatic Bearings for use in Direct Drive Linear Generators in Submerged Wave Energy Converters. In *International Conference on Ocean Energy*. Brest, France.
- CDIP. (2011). *Coastal Data Information Program*. On the WWW. (<http://cdip.ucsd.edu/>)
- Cowper, D., Kolomojcev, A., Danahy, K., & Happe, J. (2006). USCG Polar Class Aft Stern Tube Bearing Design Modifications. In *International Conference on Performance of Ships and Structures in Ice*. Banff, Canada.
- Cruz, J. (2008). *Ocean wave energy: current status and future perspectives*. Springer.
- Dean, R., & Dalrymple, R. (1991). *Water Wave Mechanics for Engineers and Scientists*. World Scientific.
- FERC. (2011). *Hydrokinetic Projects*. On the WWW. (<http://www.ferc.gov/industries/hydropower/indus-act/hydrokinetics.asp>)
- Ferrell, B. (2010). *Joint Strike Fighter Program Fielded Systems Presentation*. 2010 Annual Conference of the PHM Society.
- Floating Power Plant. (2011). (<http://floatingpowerplant.com/>)
- Gawarkiewicz, R., & Wasilczuk, M. (2007). Wear measurements of self-lubricating bearing materials in small oscillatory movement. *Wear*, 263, 458-462.

- Ginzburg, B., Tochil'nikov, D., Bakhareva, A., & Kireenko, O. (2006). Polymeric materials for water-lubricated plain bearings. *Russian Journal of Applied Chemistry*, 79, 695-706.
- Goebel, K., Saha, B., Saxena, A., Celaya, J., & Christophersen, J. (2008). Prognostics in Battery Health Management. In *Proc. IEEE*.
- Hinrichsen, D. (1999). *Coastal Waters of the World: Trends, Threats, and Strategies*. Island Press.
- Holthuijsen, L. (2007). *Waves in oceanic and coastal waters*. New York, Cambridge University Press.
- Lenee-Bluhm, P. (2010). *The Wave Energy Resource of the US Pacific Northwest*. MS Thesis, Oregon State University, Corvallis, OR.
- Marcus, K., & Allen, C. (1994). The sliding wear of ultrahigh molecular weight polyethylene in an aqueous environment. *Wear*, 178(2), 17-28.
- Marcus, K., Ball, A., & Allen, C. (1991). The effect of grinding direction on the nature of the transfer film formed during the sliding wear of ultrahigh molecular weight polyethylene against stainless steel. *Wear*, 151(2), 323-336.
- McCarthy, D. M. C., & Glavatskih, S. B. (2009). Assessment of polymer composites for hydrodynamic journal-bearing applications. *Lubrication Science*, 21(8), 331-341.
- Montgomery, D. (2009). *Design and Analysis of Experiments 7th ed.* John Wiley & Sons.
- Morison, J., O'Brien, M., Johnson, J., & Schaaf, S. (1950). The Force Exerted by Surface Waves on Piles. *Petroleum Transactions, AIME*, 189, 149-154.
- NDBC. (2011). *National Data Buoy Center*. On the WWW. (<http://www.ndbc.noaa.gov/>)
- Ocean Power Technologies. (2011). (<http://www.oceanpowertechnologies.com/>)
- Ochi, M. (1998). *Ocean waves*. Cambridge, Cambridge University Press.
- Ren, G., & Muschta, I. (2010). Challenging edge loading: A case for homogeneous polymer bearings for guidevanes. *International Journal on Hydropower and Dams*, 17(6), 121-125.
- Ruehl, K., Brekken, T., Bosma, B., & Paasch, R. (2010). Large-Scale Ocean Wave Energy Plant Modeling. In *IEEE CITERES*. Boston, MA.
- Rymuza, Z. (1990). Predicting wear in miniature steel-polymer journal bearings. *Wear*, 137(2), 211-249.
- Saha, B., Goebel, K., Poll, S., & Christophersen, J. (2009). Prognostics Methods for Batter Health Monitoring Using a Bayesian Framework. *IEEE Transactions on Instrumentation and Measurement*, 58(2), 291-296.
- Saxena, A., Celaya, J., Balaban, E., Goebel, K., Saha, B., Saha, S., et al. (2008). Metrics for Evaluating Performance Prognostic Techniques. In *International Conference on Prognostics and Health Management, Denver, CO*.
- Steele, K., & Mettlach, T. (1993). NDBC wave data - current and planned. In *Ocean Wave Measurement and Analysis - Proceedings of the Second International Symposium* (pp. ASCE, 198-207).
- Tang, L., Kacprzynski, G., Goebel, K., & Vachtsevanos, G. (2008). Methodologies for Uncertainty Management in Prognostics. In *IEEE Aerospace Conference*.
- Thordon. (2011). *SXL*. On the WWW. (<http://www.thordonbearings.com/clean-power-generation/tidalcurrentpower/design>)
- Tsuyoshi, K., Kunihiro, I., Noriyuki, H., Shozo, M., & Keisuke, M. (2005). Wear Characteristics of Oscillatory Sliding Bearing Materials in Seawater. *Journal of the Japan Institution of Marine Engineering*, 40(3), 402-407.
- Tucker, M. (1991). *Waves in Ocean Engineering: Measurement, Analysis, and Interpretation*. Ellis Horwood, LTD.
- Tucker, M., & Pitt, E. (2001). *Waves in ocean engineering*. Oxford, Elsevier.
- Uckun, S., Goebel, K., & Lucas, P. J. F. (2008). Standardizing Research Methods for Prognostics. In *International Conference on Prognostics and Health Management, Denver, CO*.
- Vachtsevanos, G., Lewis, F. L., Roemer, M., Hess, A., & Wu, B. (2006). *Intelligent Fault Diagnosis and Prognosis for Engineering Systems*. John Wiley and Sons.
- Wang, J., Yan, F., & Xue, Q. (2009). Tribological behavior of PTFE sliding against steel in sea water. *Wear*, 267, 1634-1641.
- Wave Dragon. (2011). (<http://www.wavedragon.net/>)
- Wavegen. (2011). ([http://www.wavegen.co.uk/what\\_we\\_offer\\_limpet.htm](http://www.wavegen.co.uk/what_we_offer_limpet.htm))
- W.D. Craig, J. (1964). Operation of PTFE Bearings in Sea water. *Lubrication Engineering*, 20, 456-462.
- Yemm, R. (2003). *Pelamis WEC, Full Scale Joint System Test* (Summary Report). Ocean Power Delivery Ltd. ([http://www2.env.uea.ac.uk/gmmc/energy/energy-pdfs/pelamis-joint\\_system\\_test.pdf](http://www2.env.uea.ac.uk/gmmc/energy/energy-pdfs/pelamis-joint_system_test.pdf))
- Young, I. (1999). *Wind generated ocean waves*. Netherlands, Elsevier.

**Michael T. Koopmans** is a master's student and graduate research assistant at Oregon State University, where he is employed within the Complex Engineered Systems Design Laboratory. He earned a B.S. in Mechanical Engineering from California Polytechnic State University San Luis Obispo in 2009. He has held multiple summer internships at Aperio Technologies, Solar Turbines, NASA Ames Research Center, and most recently in the embedded reasoning area at Palo Alto Research Center. His research interests include actuator prognostics, integration of system health algorithms, and applying PHM techniques to wave energy devices. Mr. Koopmans is an ASME student member and CA certified Engineer in Training.

**Stephen Meicke** is a masters student in Mechanical Engineering under Dr. Bob Paasch, researching ocean wave energy. He completed his bachelors degree in Mechanical Engineering at Virginia Tech in Blacksburg, VA in May 2009. Steves research interests lie in stress analysis, fluid-structure interaction, and finite element analysis of floating structures. His research during his first year at OSU focused on the testing of marine journal bearings for use in wave energy converters (WECs). More recently, he intends to compare strain and hydrodynamic response data taken on Columbia Power Technologies 1:7 scale Sea Ray WEC deployed in the Puget Sound, near Seattle, Washington, to response estimates obtained from simulations using LS-DYNA, a multi-physics nonlinear finite element code .

**Dr. Irem Y. Tumer** is an Associate Professor at Oregon State University, where she leads the Complex Engineered System Design Laboratory. Her research focuses on the overall problem of designing highly complex and integrated engineering systems with reduced risk of failures, and developing formal methodologies and approaches for complex system design and analysis. Her expertise touches on topics such as risk-based design, systems engineering, function-based design, failure analysis, and model-based design. Since moving to Oregon State University in 2006, her funding has largely been through NSF, AFOSR, DARPA, and NASA. Prior to accepting a faculty position at OSU, Dr. Tumer led the Complex Systems Design and Engineering group in the Intelligent Systems Division at NASA Ames Research Center, where she worked from 1998 through 2006 as Research Scientist, Group Lead, and Program Manager. She received her Ph.D. in Mechanical Engineering from The University of Texas at Austin in 1998.

**Dr. Robert Paasch** is an Associate Professor in Mechanical Engineering, and the Boeing Professor of Mechanical Engineering Design. His current research interests include the design of mechanical systems for reliability and maintainability; knowledge-based monitoring and diagnosis of mechanical systems; applications of artificial intelligence for ecological systems monitoring; and design of marine renewable energy systems. He is a member of ASME, SAE, and received his PhD from the University of California, Berkeley in 1990. Dr. Paasch's research is supported by NSF, BPA, US Navy, and USDOE.